

## COMPARISON OF DIFFERENT DRAG COEFFICIENT CORRELATIONS IN THE CFD MODELLING OF A LABORATORY-SCALE RUSHTON-TURBINE FLOTATION TANK

**Mohsen Karimi<sup>1</sup>, Guven Akdogan<sup>1</sup>, Kiran H. Dellimore<sup>2</sup>, Steven M. Bradshaw<sup>1</sup>**

<sup>1</sup> Department of Process Engineering, Stellenbosch University, Private Bag X1 Matieland 7602, Stellenbosch, South Africa.

<sup>2</sup> Department of Mechanical and Mechatronic Engineering, Stellenbosch University, Private Bag X1 Matieland 7602, Stellenbosch, South Africa.

\*Corresponding author: Mohsen Karimi, E-mail address: karimi@sun.ac.za

### ABSTRACT

Accurate specification of the drag coefficient, considering the influence of turbulence, is important in correctly predicting the air-water flow in a stirred tank. Multiphase CFD simulations in a laboratory-scale Rushton-turbine flotation tank were performed to explore the effects of four different drag coefficient correlations which were implemented in the CFD solver via user defined functions. An Eulerian-Eulerian multiphase approach with the dispersed  $k$ - $\varepsilon$  turbulence model was used to predict the gas holdup under turbulent and laminar flow conditions. Comparison of the gas holdup predictions obtained by different drag coefficient correlations showed that the choice of drag coefficient formulation significantly contributes to improving the accuracy of numerical predictions in each flow regime. The results also suggest that further improvement in the CFD simulation of stirred tanks can be achieved by better quantification of the turbulent properties associated with the interfacial forces between the continuous phase and the dispersed phase.

### NOMENCLATURE

|                  |   |
|------------------|---|
| $C_*$            | Bakker's model constant                         |
| $C_D$            | drag coefficient                                |
| $C_{D0}$         | drag coefficient for stagnant liquid            |
| $d$              | bubble diameter                                 |
| $\vec{F}_{lift}$ | lift force                                      |
| $\vec{F}_q$      | external body force                             |
| $\vec{F}_{vm}$   | virtual mass force                              |
| $\vec{g}$        | gravity vector                                  |
| $h$              | height in the vertical direction                |
| $H$              | tank height                                     |
| $\mathbf{I}$     | unit vector                                     |
| $K$              | constant (Khopkar drag coefficient correlation) |
| $K_{pq}$         | interphase momentum exchange coefficient        |
| $q$              | fluid phase                                     |
| $r$              | radial location                                 |
| $R$              | tank radius                                     |
| $Re$             | Reynolds number                                 |
| $\vec{R}_{pq}$   | interfacial force                               |
| $Stk$            | Stokes number                                   |
| $S_q$            | mass source term                                |
| $t$              | time  |
| $T_L$            | integral time scale                             |
| $U_S$            | slip velocity                                   |

|               |                                 |
|---------------|---------------------------------|
| $U_T$         | particle terminal velocity      |
| $\vec{U}_q$   | mean velocity vector            |
| $\vec{v}$     | phase velocity                  |
| $y^+$         | dimensionless wall distance     |
| $\alpha_q$    | volume fraction of phase $q$    |
| $\varepsilon$ | relative error                  |
| $\lambda$     | Kolmogorov length scale         |
| $\mu_T$       | turbulent viscosity             |
| $\mu$         | laminar viscosity               |
| $\tau$        | particle/bubble relaxation time |
| $\nu$         | kinematic viscosity             |
| $\rho$        | fluid density                   |

### INTRODUCTION

Mechanically agitated tanks are widely used in the mineral processing industry to perform flotation-separation processes. The uniform distribution of the injected air from the sparger and its total holdup (i.e., the volume fraction of air) inside the flotation tank are important, since they strongly influence the efficient collision and attachment of solid particles and air bubbles in the tank. This in turn enhances the overall flotation recovery. One attractive approach for investigating the fully turbulent multiphase flow behaviour of the air and water phases inside of a flotation tank is computational fluid dynamics (CFD). Several studies have demonstrated that CFD is capable of modelling the principal hydrodynamics inside the tank, including the air distribution and its holdup (Dong et al., 1994, Ranade and Van den Akker, 1994, Bakker and Van den Akker, 1994, Lane et al., 2000). The accurate prediction of the air phase distribution is dependent upon the correct modelling of the interfacial forces between the different phases inside the tank (i.e., water as the continuous phase and air as the dispersed phase). It has also been shown that of the various interfacial forces, the drag force is the most significant one influencing the air bubbles (Brucato et al., 1998, Lane et al., 2002, Lane et al., 2005, Khopkar and Ranade, 2006). The slip velocity of the air bubbles arises from the balance between the drag and the buoyancy forces which in turn determine the air distribution and its holdup. Hence, a drag coefficient correlation incorporating the influence of the turbulent eddies on the air bubbles is essential to the accurate numerical prediction of the liquid and gas phases inside a Rushton-turbine flotation tank.

The most commonly used drag coefficient correlations have been empirically derived from measurements of a single particle rising or falling in a stagnant liquid in the

absence of turbulent effects on the dispersed phase. For instance, the standard drag coefficients proposed by Schiller and Naumann (Schiller and Naumann, 1935) and by Ishii and Zuber (Ishii and Zuber, 1979) do not consider the role of turbulence (e.g., caused by the impeller rotation in the stirred tank) on the drag force. In many CFD simulations of stirred tanks, interfacial forces between the continuous and the dispersed phases have been modelled by using either the Ishii-Zuber or Schiller-Naumann correlations for the drag force (Morud and Hjertager, 1996, Kerdouss et al., 2006). However, over the past twenty years many attempts have been made to integrate the effects of turbulence on the bubble dispersion into drag coefficient correlations for stirred tanks. One of the earliest efforts to incorporate the effect of turbulent eddies on the dispersed phase flow pattern in a stirred tank was made by Bakker (Bakker, 1992). He introduced a modified bubble Reynolds number in which an adjustable fraction of the turbulent eddy viscosity was included to account for the effect of turbulence on the drag force. Bakker's numerical predictions showed that the maximum gas holdup occurs close to the sparger. Later, in 1998 Brucato et al. (Brucato et al., 1998) performed experiments to measure solid particle settling velocities and drag coefficients in a turbulent flow field. Based on these measurements they proposed a new correlation which relates the drag coefficient to the ratio of the particle size and Kolmogorov turbulent length scale. Subsequently, in 2002 a CFD based method for the multiphase modelling of the mechanically stirred tank was developed by Lane et al. (Lane et al., 2002). They applied Brucato's model to interpret the interaction between the air phase and turbulent eddies. They also continued the development of the CFD methodology for the stirred tank and in 2005 Lane et al. (Lane et al., 2005) proposed a new drag coefficient correlation which was based on the available experimental data from the literature (Spelt and Biesheuvel, 1997, Brucato et al., 1998, Poorte and Biesheuvel, 2002). Lane et al. showed that the drag coefficient is associated with the ratio of the turbulent to stagnant terminal velocity. Khopkar et al. (Khopkar and Ranade, 2006) also applied the proposed drag coefficient correlation of Brucato and confirmed that the drag coefficient is a function of particle size and the Kolmogorov length scale. However, they found that a constant with a smaller magnitude matched their predictions with experiments. Another notable study focusing on the influence of turbulence on the drag force was performed by Doroodchi et al. (Doroodchi et al., 2008). They explored the role of dispersed phase density and size on the drag force by conducting experiments using an oscillating turbulence generator. Their experiments yielded trends which were similar to the trend produced by the Lane et al. correlation for the drag coefficient. Nevertheless, the operational conditions (i.e., the velocity ratio and Stokes number) caused a significant quantitative discrepancy between the experimental data and the drag coefficient correlation of Lane. They also suggested that when the turbulence is dominant, a drag coefficient correlation incorporating the Richardson number should be used.

It is important to note here that all of the above mentioned correlations for the drag coefficient have been developed under different flow conditions and may therefore require modification when applied outside of the operational range under which they were formulated. It is therefore useful to evaluate the predictive capability of each drag

coefficient under similar laminar as well turbulent conditions. The aim of this work is to compare the performance of four different drag coefficient correlations under laminar and turbulent conditions in the CFD modelling of the water and air phases inside a laboratory-scale Rushton-turbine flotation tank.

## GOVERNING EQUATIONS

In order to compare the different drag coefficient correlations, the flow of air and water in a laboratory-scale Rushton-turbine flotation tank based on the geometry of Newell (Newell, 2006) was modelled using an Eulerian-Eulerian multiphase model. In this approach the conservation of mass and momentum equations for each phase,  $q$ , were solved:

$$\begin{aligned} \frac{\partial}{\partial t}(\alpha_q \rho_q) + \nabla \cdot (\alpha_q \rho_q \vec{U}_q) &= S_q \quad (1) \\ \frac{\partial}{\partial t}(\alpha_q \rho_q \vec{U}_q) + \nabla \cdot (\alpha_q \rho_q \vec{U}_q \vec{U}_q) &= -\alpha_q \nabla p + \alpha_q \rho_q \vec{g} + \nabla \cdot \\ &(\alpha_q \mu_q (\nabla \vec{v}_q + \nabla \vec{v}_q^T) + \alpha_q (\mu_T - \frac{2}{3} \mu_q) \nabla \cdot \vec{v}_q \mathbf{I}) + \\ &\sum_{p=1}^n \vec{R}_{pq} + \vec{F}_q + \vec{F}_{lift} + \vec{F}_{vm} \quad (2) \end{aligned}$$

where  $\alpha_q$  is the volume fraction of phase  $q$ ,  $\rho_q$  is the density,  $\vec{U}_q$  is the mean velocity vector,  $S_q$  is the mass source term (e.g. a source of air at the sparger),  $p$  is the pressure,  $\vec{g}$  is the gravity vector,  $\mu_q$  is the laminar viscosity,  $\mu_T$  is the turbulent viscosity,  $\mathbf{I}$  is the unit vector,  $\vec{v}$  is the phase velocity,  $\vec{R}_{pq}$  is the interfacial force,  $\vec{F}_q$  is the external body force (e.g. the Coriolis and the centrifugal force caused by rotation of impeller),  $\vec{F}_{lift}$  is the lift force, and  $\vec{F}_{vm}$  is the virtual mass force.

Previous studies (Lane et al., 2002, Khopkar and Ranade, 2006) have suggested that the influence of the virtual mass force and the lift force on the air bubbles inside the stirred tank is negligible. Therefore, in this paper it is assumed that  $\vec{F}_{vm}$  and  $\vec{F}_{lift}$  are zero. However, it is necessary to obtain an expression for the interfacial force,  $\vec{R}_{pq}$ , in order to close Eq. (2). This was achieved using the following equation (ANSYS FLUENT, 2009):

$$\sum_{p=1}^n \vec{R}_{pq} = \sum_{p=1}^n K_{pq} (\vec{v}_p - \vec{v}_q) \quad (3)$$

where  $K_{pq}$  denotes the interphase momentum exchange coefficient which can be expressed as:

$$K_{pq} = \frac{3}{4} \rho_q \alpha_q \alpha_p \frac{C_D}{d_p} |\vec{v}_p - \vec{v}_q| \quad (4)$$

In Eq. (4),  $C_D$  is the drag coefficient and  $d_p$  is the bubble diameter.

As noted in the introduction, the drag coefficient is modelled using an empirical correlation. In this study four different correlations for  $C_D$  were evaluated. The first one, which was developed for laminar flow, is the standard Schiller-Naumann (Schiller and Naumann, 1935):

$$C_D = \begin{cases} \frac{24(1+0.15Re^{0.687})}{Re} & Re \leq 1000 \\ 0.44 & Re > 1000 \end{cases} \quad (5)$$

where  $Re$  is the relative Reynolds number for the continuous phase ( $q$ ) and the dispersed phase ( $p$ ):

$$Re = \frac{\rho_q |\vec{v}_p - \vec{v}_q| d_p}{\mu_q} \quad (6)$$

Bakker (Bakker, 1992) modified the Reynolds number expression in Eq. (6) to include the effect of turbulent eddies on the air bubbles by adding an adjustable fraction of the turbulent viscosity. This yielded a new drag coefficient correlation which can be expressed as follows:

$$Re = \frac{\rho_q |\vec{v}_p - \vec{v}_q| d_p}{\mu_q + C_s \times \mu_T} \quad (7)$$

In Eq. (7),  $C_*$  is a constant which accounts for the reduction in the slip velocity of the air bubbles when they are moving in the turbulent flow field of the stirred tank. Bakker recommended a value of 0.02 for the  $C_*$ , however, this value can be varied based on the conditions simulated. The third drag coefficient correlation evaluated was proposed by Khopkar et al. (Khopkar and Ranade, 2006), who modified Brucato's model (Brucato et al., 1998) which is based on experimental measurements of the average particle settling velocity under turbulent flow conditions. Brucato et al. correlated the experimental drag coefficients with the ratio of particle/bubble size to the Kolmogorov length scale:

$$\frac{C_D - C_{D0}}{C_{D0}} = K \left( \frac{d_p}{\lambda} \right)^3 \quad (8)$$

where  $C_{D0}$  is the drag coefficient in the stagnant liquid, and  $K$  is the correlation constant. Brucato reported this value to be  $8.76 \times 10^{-4}$ , while Khopkar reduced this constant to  $6.5 \times 10^{-6}$ .  $\lambda$  is the Kolmogorov length scale:

$$\lambda = \left( \frac{\nu^3}{\varepsilon} \right)^{1/4} \quad (9)$$

where  $\varepsilon$  is the turbulent dissipation rate and  $\nu$  is the kinematic viscosity.

The fourth drag coefficient correlation evaluated was proposed by Lane (Lane, 2006) based on a curve fit of the available experimental stirred tank drag coefficient data from the literature. Lane found that there is a relationship between the ratio of the slip velocity ( $U_s$ ) to the particle terminal velocity ( $U_T$ ) and the drag coefficient as follows:

$$\frac{C_D}{C_{D0}} = \left( \frac{U_s}{U_T} \right)^{-2} \quad (10)$$

where the ratio of  $U_s/U_T$  depends on the Stokes number:

$$\frac{U_s}{U_T} = 1 - 1.4Stk^{0.7} \exp(-0.6Stk) \quad (11)$$

And the Stokes number is defined as:

$$Stk = \frac{\tau_p}{T_L} \quad (12)$$

In Eq. (12)  $\tau_p$  represents the particle relaxation time and  $T_L$  is the integral time scale. The relaxation time for the bubbles ( $\tau_b$ ) can be calculated using the following:

$$\tau_b = \frac{U_T}{2g} \quad (13)$$

In Eq. (13)  $T_L$  represents the turbulent characteristics of the flow which can be expressed as:

$$T_L = 0.135 \frac{k}{\varepsilon} \quad (13)$$

where  $k$  is the turbulent kinetic energy and  $\varepsilon$  is the turbulent dissipation rate.

In this paper the standard Schiller-Naumann, Bakker, Khopkar and Lane drag coefficient correlations have been compared to predict the gas holdup and the gas distribution in a Rushton-turbine flotation tank under laminar (0 rpm) and turbulent (350 rpm) conditions.

## NUMERICAL APPROACH

To compare the effects of various drag coefficient correlations in the modelling of the stirred tank, a 2.25 L stirred vessel based on the geometry reported by Newell (Newell, 2006) was modelled. The 145mm diameter tank is fully baffled and is equipped with a 6-bladed impeller mounted on a central disk (Figure 1).

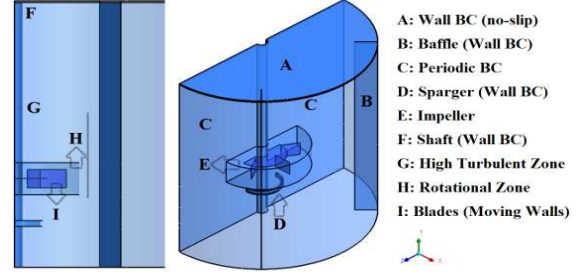


**Figure 1:** Schematic illustration of the laboratory-scale Rushton-turbine flotation tank showing the boundary conditions used in all simulations.

Figure 1 schematically shows the boundary conditions used in all simulations. In order to model the impeller rotation, the tank was divided into a bulk and a rotational zone. The multiple reference frames method was implemented to solve the governing equations in both the stationary and rotating reference frames. An angular velocity of zero, relative to the rotational zone, was defined for the blades to model their rotation. In addition, air was introduced into the vessel using a mass source at the sparger, while a no-slip velocity boundary condition was applied at the sparger. Only half of the geometry of the tank was modelled in order take advantage of rotational symmetry and reduce computational time. It was therefore necessary to prescribe periodic boundary conditions at the left and right walls of the computational domain. At the other boundaries, including the baffles and the outer walls, a no slip boundary condition and standard wall functions were applied.

The computational domain was discretised into 235,872 hexagonal elements with finer grid resolution in the vicinity of the impeller. A maximum skewness ratio of 0.45 was applied to ensure good mesh quality. In addition,  $y^+$  (i.e., the dimensionless wall distance) was constrained within the logarithmic law layer (i.e.,  $30 < y^+ < 300$ ) to capture temporal turbulent fluctuations.

All simulations were performed on the Stellenbosch University High Performance Computing cluster with 8 nodes and an installed capacity of 2.83GHz processors per node with 16GB of RAM. The Eulerian-Eulerian multiphase equations in conjunction with the dispersed k- $\varepsilon$  turbulence model were solved using ANSYS Fluent. The four different drag coefficient correlations were implemented in the numerical model via user defined functions (UDFs). The SIMPLE scheme was used to couple the continuity and momentum equations to derive the pressure field. A second order upwind discretization method was used for the momentum equations, while the volume fraction equation was computed using the QUICK method. Solutions were assumed to be converged when the normalized residual for the continuity was less than  $1 \times 10^{-3}$  and the predicted gas holdup varied by a difference of less than 1% between the final gas holdup value and the average value for the last five seconds of flow time.

## RESULTS AND DISCUSSION

In order to investigate the performance of the four different drag coefficient correlations (i.e., the standard Schiller-Naumann, Bakker, Khopkar and Lane correlations), two different angular velocities of the impeller, 0 rpm and 350 rpm (corresponding to the laminar and the turbulent flow regimes) were considered.

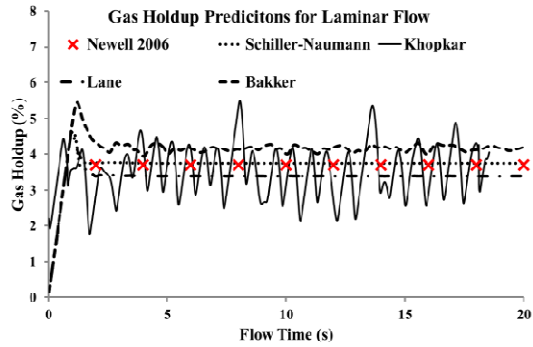


**Figure 2:** Comparison of different drag coefficients for laminar flow at 0 rpm.

The gas holdup predictions from the four different drag coefficient correlations are compared in Figure 2 as a function of flow time. The symbols indicate the experimental data from Newell (Newell, 2006), the dotted line corresponds to the predictions for the Schiller-Naumann model, the solid line to the predictions from the Khopkar model, the dashed-dotted line to the Lane model and the dashed line to the Bakker model. The results show that applying different correlations for the drag coefficients can significantly affect the predicted gas holdup. The drag coefficient equations incorporating the turbulent effects yield only a fair agreement with the experimental data. The Bakker model overpredicts the gas holdup by an average difference of less than 14.9%, while the Lane model underpredicts the gas holdup by an average difference of less than 8.7%. Figure 2 also clearly demonstrates that of the four drag coefficient correlations evaluated the Khopkar model does not meet the second convergence criterion (i.e., the negligible variations of the gas holdup predictions), even though the continuity residual is less than  $1 \times 10^{-3}$ . This can be attributed to the differences in the description of the turbulent dissipation rate ( $\epsilon$ ) in Eq. (9) between the Khopkar model and its implementation in this paper. In the Khopkar drag coefficient correlation an average value of  $\epsilon$  was used to compute the Kolmogorov length scale, while in the current study the implemented UDF utilizes local values of  $\epsilon$ . The gas holdup predicted by the Schiller-Naumann correlation, however, matches the experiment very closely, within an average difference of 1.4%. These results are consistent with expectation since the Schiller-Naumann drag coefficient correlation is the only model in this study that has been developed for the laminar flow while the other models are turbulent formulations.

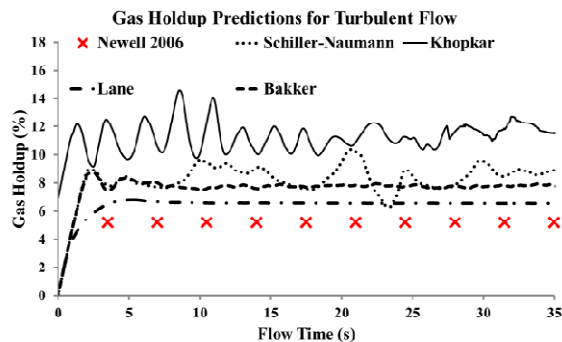
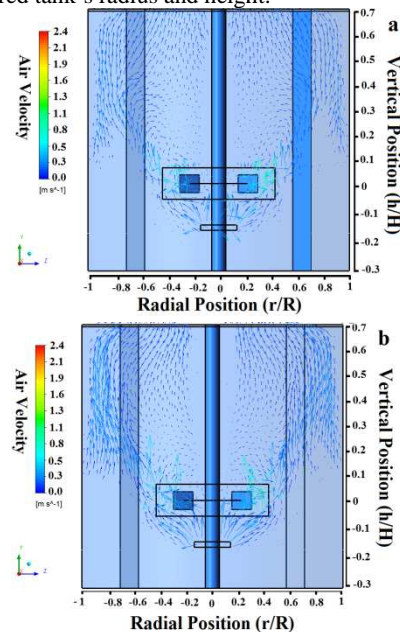


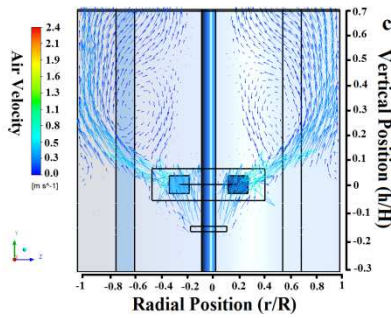
**Figure 3:** Comparison of different drag coefficient correlations for turbulent flow at 350 rpm.

The numerical predictions of the gas holdup for the turbulent flow as a function of flow time have been shown in Figure 3. In this figure the symbols indicate the

experimental data from Newell (Newell, 2006), the dotted line corresponds to the Schiller-Naumann model, the solid line corresponds to the gas holdup predictions for the Khopkar model, the dashed-dotted line to the Lane model, and the dashed line to the predictions of Bakker model. The figure shows that all of the implemented models overpredict the gas holdup. In addition, the results presented for the Khopkar model indicate that a converged solution was not obtained (as seen in the laminar case). The numerical predictions from the Schiller-Naumann model yielded poor agreement (an average difference of  $< 68.7\%$ ) with the experimental data, while those from the Bakker and Lane models showed fair agreement with the experimental data (average differences of less than 48.1% and 25.2% for the Bakker and Lane models, respectively). This suggests that in developing a CFD methodology for the stirred tank the influence of turbulent eddies on the drag force should be taken into account. Based on these results it can be concluded that by incorporating the effect of turbulence on the air bubbles through the modification of the drag coefficient correlation the prediction of gas holdup can be significantly improved. The Lane model produced the closest agreement with the data, however, the observed discrepancy between the numerical predictions and the experimental measurements is not negligible and might be reduced by modifying the drag coefficient correlation to include the Richardson number following the suggestion of Doroodchi et al. (Doroodchi et al., 2008).

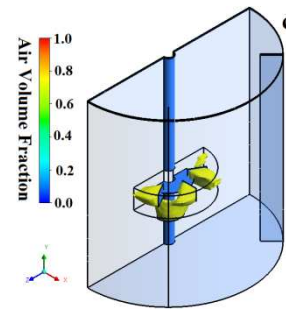
To gain further insight into the dispersed phase hydrodynamics Figure 4 compares the vector plots of the air phase computed using the three most stable drag coefficient correlations (Schiller-Naumann, Bakker, and Lane) on a vertical cross-section through the stirred tank at 350 rpm. The predictions by the Khopkar model were excluded because diverged solutions were obtained under both laminar and turbulent conditions. In this figure  $r$  and  $h$  represent the spatial coordinates while  $R$  and  $H$  indicate the stirred tank's radius and height.





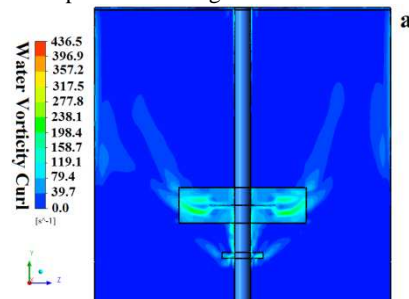
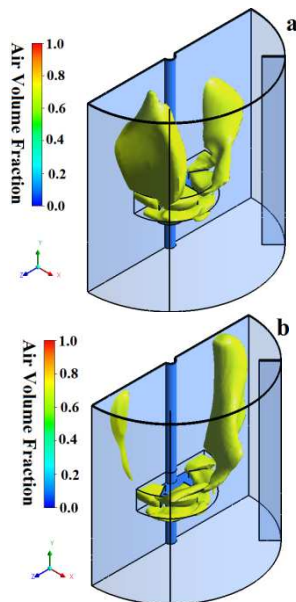
**Figure 4:** Comparison of the air velocity vectors for the drag coefficient correlations of: (a) Schiller-Naumann, (b) Bakker, and (c) Lane, at 350 rpm.

The applied drag coefficient equations are able to predict the overall air flow pattern inside the stirred tank. In all cases the air injected from the sparger has an upward movement towards the impeller. Due to the rotation of the impeller, the air is accelerated around the rotational zone ( $-0.4 < r/R < 0.4$ ,  $-0.05 < h/H < 0.05$ ) while near the top of the tank the dispersed phase velocity is decreased. The predicted air velocity magnitude from the Schiller-Naumann and Bakker drag coefficient correlations in the bulk flow region ( $-1.0 < r/R < 1.0$ ,  $0.2 < h/H < 0.7$ ) are similar, while the velocity predicted by Lane's model is slightly higher. The figure also shows that a symmetric vortex flow pattern of air is formed near the top of the impeller. The distribution of this vortex varies slightly depending on the drag coefficient correlation used. The Schiller-Naumann and Bakker models capture this vortex pattern close to the rotational zone (within the range  $0.3 < r/R < 0.5$ ,  $0 < h/H < 0.15$  for the Schiller-Naumann and  $0.2 < r/R < 0.4$ ,  $0.1 < h/H < 0.25$  for the Bakker model), while from the Lane model's predictions, the vortex occurs near the bulk region of the tank (within the range  $0.4 < r/R < 0.8$ ,  $0.2 < h/H < 0.4$ ).



**Figure 5:** Comparison of the air cavity location for the drag coefficient correlations of: (a) Schiller-Naumann, (b) Bakker, and (c) Lane, at 350 rpm.

The formation of the air cavity in the multiphase flow of the stirred tank behind the impeller blades is a well-known phenomenon. It can be attributed to the presence of a substantial pressure gradient in this region due to the rotation of the impeller. The formation of air cavities behind the impeller blades of a stirred tank has been numerically investigated by Lane (Lane, 2006). He showed that a ventilated cavity forms in the trailing vortices behind the blades. In the current study the prediction of the air cavity's location, is used to evaluate the predictive performance of each drag coefficient correlation. It is assumed here that the regions in the computational domain with an air volume fraction greater than 80% indicate the formation of an air cavity. These cavities are illustrated by iso-surfaces of the air phase in which the air volume fraction is equal to or greater than 0.8 as shown in Figure 5. This figure clearly shows that using different drag coefficient correlations can have a significant impact on the prediction of the air distribution and the air cavity's location in the stirred tank. The drag coefficients of Schiller-Naumann and Bakker (Figure 5 a and b) predict a high volume fraction of the air in the bulk flow region. In contrast, under the same conditions applying the Lane drag coefficient correlation (Figure 5 c) results in the accumulation of air behind the impeller blades. This latter result is consistent with expectation and with the observations reported in previous studies (Lane, 2006, Vivek et al., 1998). Based on these results it can be concluded that the Lane model's more accurate prediction of the distribution of the air and water phases in the stirred tank is due to its more sophisticated treatment of the influence of turbulence on bubble dispersion. Further insight into the distribution of the dispersed phase can be gained by considering the vorticity flow field in the stirred tank which is presented in Figure 6.



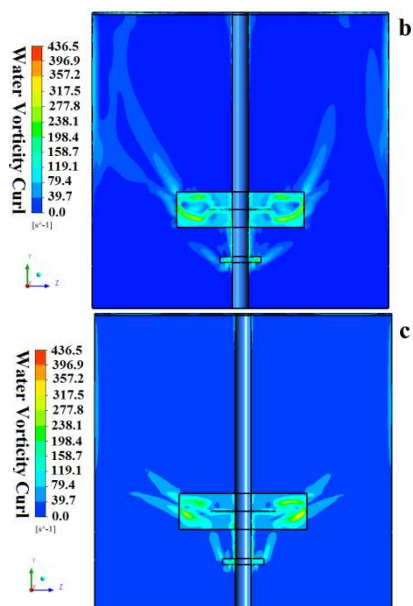


**Figure 6:** Comparison of the vorticity contours for the drag coefficient correlations of: (a) Schiller-Naumann, (b) Bakker, and (c) Lane, at 350 rpm.

Figure 6 shows contour plots of the vorticity magnitude (i.e., the measure of local rotation in the fluid) for the three different drag coefficient correlations at 350 rpm. In the three cases shown the maximum vorticity occurs in the rotational zone, as expected, due to the impeller rotation. The vorticity contours predicted by the Schiller-Naumann correlation in the bulk flow region (Figure 6a) form a symmetric pattern inside the tank. This is comparable to the symmetric pattern for accumulation of air in the bulk region of the stirred tank seen in Figure 5a. From this it can be inferred that the inaccurate estimation of the location of the air cavity by the (laminar) Schiller-Naumann model may be associated with its underprediction of the vorticity distribution in the water phase, which suggests that the air does not disperse as rapidly as it does in a well-mixed (turbulent) stirred tank. The contour plots of vorticity predicted by Bakker's model, however, illustrate an asymmetric vorticity distribution above the impeller zone (Figure 6b) which is similar to the observed asymmetric iso-surface of air seen in Figure 5b. This can be explained by the uneven vorticity distribution observed in the bulk region of the tank which suggests that the air dispersion is more rapid on one side of the impeller. This leads to the asymmetric accumulation of air in the bulk flow region of the tank seen in Figure 5b. This result suggests that the modification of the Reynolds number formulation in Bakker's model is not able to adequately predict the effect of turbulent vortices on the dispersed phase hydrodynamics. Figure 6c shows the vorticity contour plots predicted by the Lane drag coefficient correlation. The vorticity distribution (Figure 6c) and the air cavity location (Figure 5c) predicted by Lane's model follow very similar patterns. The high vorticity magnitude (which is 43% greater than predicted by the Schiller-Naumann and Bakker models) in the vicinity of the impeller blades promotes rapid dispersion of the air thereby preventing the formation of air cavities in the bulk flow region of the tank. This is consistent with the observations reported in previous studies (Lane, 2006, Vivek et al., 1998).

## CONCLUSION

The air and water flow inside a laboratory-scale Rushton-turbine flotation tank was numerically modelled using an Eulerian-Eulerian approach to explore the influence of different drag coefficients on the dispersed phase behaviour. Four different drag coefficient correlations including the Schiller-Naumann, Bakker, Khopkar and Lane models were implemented via user defined functions in the CFD solver to estimate the gas holdup under laminar and turbulent conditions. The numerical predictions of the gas holdup for laminar flow showed that the drag coefficient correlation which was formulated for the stagnant liquid provided a better match (within an average difference of 1.4%) to the experimental data. The turbulent flow results showed the Lane model produced the closest agreement with the experiment, however, the observed discrepancy between the numerical predictions and the experimental data is not negligible (within an average difference of 25.2%) and might be reduced by modifying the drag coefficient correlation to include the Richardson number. Overall the results presented here suggest that further improvement in the CFD simulation of stirred tanks can be achieved by better quantification of the turbulent properties associated with the interfacial forces between the continuous phase and the dispersed phase.

## ACKNOWLEDGMENT

This work was supported by the Overarching Strategic Funding scheme from Stellenbosch University in South Africa.

## REFERENCES

- ANSYS FFLUENT 2009. *User's Guide*, Canonsburg, PA, ANSYS, Inc.
- BAKKER, A. 1992. *Hydrodynamics of Stirred Gas-Liquid Dispersions*. PhD, Technical University of Delf.
- BAKKER, A. & VAN DEN AKKER, H. E. A. 1994. A Computational Model for Gas-Liquid Flow in Stirred Reactors. *TransIChemE*, 72, 573-582.
- BRUCATO, A., GRISAFI, F. & MONTANTE, G. 1998. Particle drag coefficients in turbulent fluids. *Chemical Engineering Science*, 53, 3295-3314.
- DONG, L., JOHANSEN, S. T. & ENGH, T. A. 1994. Flow induced by an impeller in an unbaffled tank—II. Numerical modelling. *Chemical Engineering Science*, 49, 3511-3518.
- DOROODCHI, E., EVANS, G. M., SCHWARZ, M. P., LANE, G. L., SHAH, N. & NGUYEN, A. 2008. Influence of turbulence intensity on particle drag coefficients. *Chemical Engineering Journal*, 135, 129-134.
- ISHII, M. & ZUBER, N. 1979. Drag coefficient and relative velocity in bubbly, droplet or particulate flows. *AIChE Journal*, 25, 843-855.
- KERDOUSS, F., BANNARI, A. & PROULX, P. 2006. CFD modeling of gas dispersion and bubble size in a double turbine stirred tank. *Chemical Engineering Science*, 61, 3313-3322.
- KHOPKAR, A. R. & RANADE, V. V. 2006. CFD simulation of gas-liquid stirred vessel: VC, S33, and L33 flow regimes. *AIChE Journal*, 52, 1654-1672.
- LANE, G. L. 2006. *Computational Modelling of Gas-Liquid Flow in Stirred Tanks*. PhD, University of Newcastle

- LANE, G. L., SCHWARZ, M. P. & EVANS, G. M. Comparison of CFD methods for modelling of stirred tanks. 10th European Conference on Mixing, 2000 Delf, Netherlands. 273-280.
- LANE, G. L., SCHWARZ, M. P. & EVANS, G. M. 2002. Predicting gas-liquid flow in a mechanically stirred tank. *Applied Mathematical Modelling*, 26, 223-235.
- LANE, G. L., SCHWARZ, M. P. & EVANS, G. M. 2005. Numerical modelling of gas-liquid flow in stirred tanks. *Chemical Engineering Science*, 60, 2203-2214.
- MORUD, K. E. & HJERTAGER, B. H. 1996. LDA measurements and CFD modelling of gas-liquid flow in a stirred vessel. *Chemical Engineering Science*, 51, 233-249.
- NEWELL, R. 2006. *Hydrodynamics and scale-up in rushton turbine flotation cells*. PhD, Univeristy of South Australia.
- POORTE, R. E. G. & BIESHEUVEL, A. 2002. Experiments on the motion of gas bubbles in turbulence generated by an active grid. *Journal of Fluid Mechanics*, 461, 127-154.
- RANADE, V. V. & VAN DEN AKKER, H. E. A. 1994. A computational snapshot of gas-liquid flow in baffled stirred reactors. *Chemical Engineering Science*, 49, 5175-5192.
- SCHILLER, L. & NAUMANN, Z. 1935. Ver. Deutsch Ing.
- SPELT, P. D. M. & BIESHEUVEL, A. 1997. On the motion of gas bubbles in homogeneous isotropic turbulence. *Journal of Fluid Mechanics*. *Journal of Fluid Mechanics*, 336, 221-244.
- VIVEK, V. R., VAIBHAV, R. D. & VIA, C. 1998. GAS-LIQUID FLOW IN STIRRED REACTORS: Trailing Vortices and Gas Accumulation behind Impeller Blades.

, Newport Beach, USA.